



Article

Electrical Discharge Machining of Al₂O₃ Using Copper Tape and TiO₂ Powder-Mixed Water Medium

Sergey N. Grigoriev ¹, Anna A. Okunkova ^{1,*}, Marina A. Volosova ¹, Khaled Hamdy ^{1,2}
and Alexander S. Metel ¹

¹ Department of High-Efficiency Processing Technologies, Moscow State University of Technology STANKIN, Moscow 127055, Russia

² Production Engineering and Mechanical Design Department, Faculty of Engineering, Minia University, Minia 61519, Egypt

* Correspondence: a.okunkova@stankin.ru; Tel.: +7-909-913-12-07

Abstract: Aluminum-based ceramics are used in industry to produce cutting tools that resist extreme mechanical and thermal load conditions during the machining of Ni-based and high-entropy alloys. There is wide field of application also in the aerospace industry. Microtexturing of cutting ceramics reduces contact loads and wear of cutting tools. However, most of the published works are related to the electrical discharge machining of alumina in hydrocarbons, which creates risks for the personnel and equipment due to the formation of chemically unstable dielectric carbides (methanide Al₃C₄ and acetylenide Al₂(C₂)₃). An alternative approach for wire electrical discharge machining Al₂O₃ in the water-based dielectric medium using copper tape of 40 μm thickness and TiO₂ powder suspension was proposed for the first time. The performance was evaluated by calculating the material removal rate for various combinations of pulse frequency and TiO₂ powder concentration. The obtained kerf of 54.16 ± 0.05 μm in depth demonstrated an increasing efficiency of more than 1.5 times with the closest analogs for the workpiece thickness up to 5 mm in height. The comparison of the performance (0.0083–0.0084 mm³/s) with the closest analogs shows that the results may correlate with the electrical properties of the assisting materials.

Keywords: alumina; assisting coating; brass wire; cutting ceramic; electrical discharge machining; electrode; erosion; insulating; microtexturing; sublimation



Citation: Grigoriev, S.N.; Okunkova, A.A.; Volosova, M.A.; Hamdy, K.; Metel, A.S. Electrical Discharge Machining of Al₂O₃ Using Copper Tape and TiO₂ Powder-Mixed Water Medium. *Technologies* **2022**, *10*, 116. <https://doi.org/10.3390/technologies10060116>

Academic Editor: Manoj Gupta

Received: 25 October 2022

Accepted: 7 November 2022

Published: 11 November 2022

Publisher's Note: MDPI stays neutral with regard to jurisdictional claims in published maps and institutional affiliations.



Copyright: © 2022 by the authors. Licensee MDPI, Basel, Switzerland. This article is an open access article distributed under the terms and conditions of the Creative Commons Attribution (CC BY) license (<https://creativecommons.org/licenses/by/4.0/>).

1. Introduction

Cutting ceramics are used in industry to produce cutting tools that resist extreme mechanical and thermal load conditions during the machining of Ni-based and high-entropy alloys [1–4] due to achieving temperatures up to 800 °C in the contact area and other specific properties of these materials [5–7]. The wide field of applications includes the aerospace, automotive, chemistry and nuclear industries [8–11]. In cutting tools, microtexturing of cutting ceramics reduces contact loads and significantly reduces the wear of cutting tools and coatings [12–14]. Microtexturing is often provided by a different group of the machining technologies, such as:

- Chemical and electrochemical processing, including chemical etching and electrochemical machining [15,16];
- Mechanical processing with a cutting tool or hydroabrasive jet [17,18];
- Thermal ablation process based on laser, electron beam, and electrical erosion of the materials [19–23].

Electrical discharge machining has multiple known advantages related to the physics of the process and geometrical features:

- Ability to work with the preproduced electrode of any shape that allows microtexturing in one single approach of the electrode tool to the workpiece (sinking) [24–26];

- Ability to produce high-precision linear surfaces by a constantly rewinding electrode tool that excludes any influence of the tool wear on the tolerance of the shaping [27,28];
- Low tool wear rate that is especially relevant in the case of sinking in comparison with other technologies using a preproduced tool where the operational life of the tool can count by a few minutes that often requires multilayer and nanocoatings [29–32];
- Ability to process the material despite their hardness and viscosity (in the case of aluminum and titanium alloys, composites) [33–36];
- Accuracy up to 80–100 nm due to the use of the new class of linear engines [37,38];
- Ability to perform electrical and acoustic monitoring of process efficiency [39,40].

The problem of applying electrical discharge machining methods to the dielectric materials such as cutting ceramics such as Al_2O_3 , AlN , SiAlON , Si_3N_4 , ZrO_2 , etc., is in the absence of required electrical properties of these materials [41–46]. That can be solved by adding a conductive phase into the ceramic structure of the sintered composite [47–49] that influence as well on the physical and mechanical properties of a new material depending on the conductive and main material fraction or by adding assisting conductive coating or powder in the working area [50,51]. The method was first proposed and patented in 1986 by Russian scientists [52]. In this context, electrical discharge machining of ZrO_2 ceramic in hydrocarbons showed the most outstanding results [53–57] that can be related to the thermochemical properties of this material when thermodissociated Zr^{4+} and metal-like carbide ZrC (delocalized metal bond d-element carbide) exhibit similar electrical conductivity ($\leq 44.1 \mu\Omega\cdot\text{cm}$ at a normal temperature depending on purity) and assists processing [58,59]. However, the works published on other ceramics do not show any significant advances in efficiency-maximal depth of 1693 μm from the coating surface after 150 min of processing by the copper-tungsten electrode of $\text{Ø}308 \mu\text{m}$ for AlN , for example [46,60–62].

It should be noted that the published works are related to the electrical discharge machining of alumina in hydrocarbons [51,63–66], where obviously during thermochemical dissociation of Al_2O_3 [67,68], released aluminum ion Al^{3+} binds with dissociation products of hydrocarbon to form methanide Al_3C_4 and acetylenide $\text{Al}_2(\text{C}_2)_3$ [44,68–70]. In other words, it leads to the formation of chemically unstable dielectric carbides exhibiting dielectric properties that not only hampers processing but also creates risks for personnel and equipment.

The alternative combined approach for wire electrical discharge machining of Al_2O_3 in the water-based dielectric medium was proposed for the first time (Figure 1).

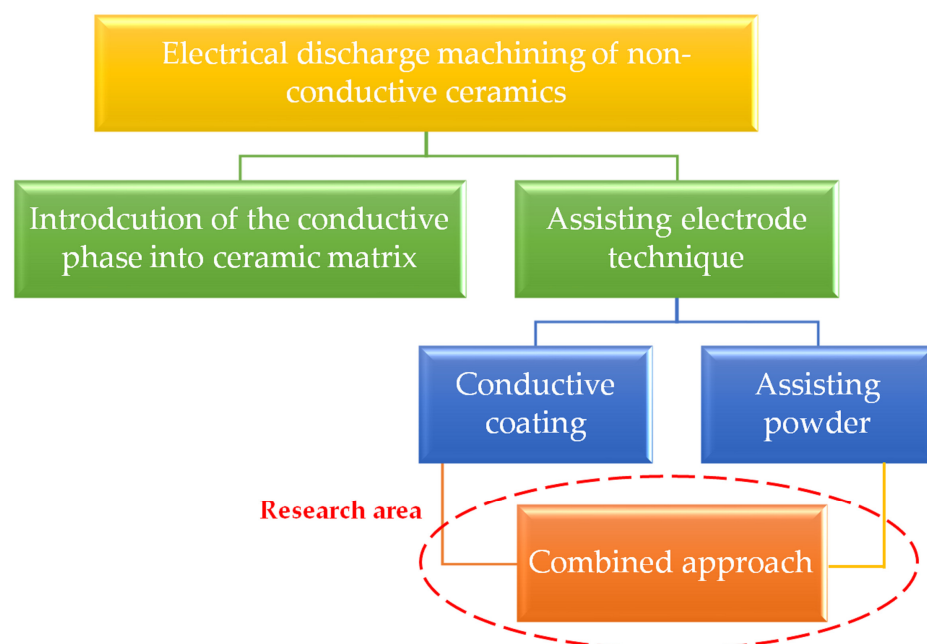


Figure 1. Existing methods of electrical discharge machining of non-conductive ceramics.

Deionized water was chosen as a basis for assisting powder fluid to avoid formation of the mentioned carbides. Powder-mixed electric discharge machining (PMEDM) was first developed as an advanced technique to improve machining productivity [71–73]. The use of powder material reduces dielectric medium strength, creating a more uniform density of the electrical discharge at low pulse energy (Figure 2a–c), reducing surface roughness, improving productivity, and reducing tool electrode wear compared with conventional electrical discharge machining. A powder material (micro- or nano-sized) of titanium dioxide, cesium dioxide, and other ceramic components is introduced into the working area (interelectrode gap), which, upon reaching the temperatures of the discharge channel, would acquire better conductive properties (Figure 3) and provoke denser discharges of pulses during processing conductive materials. It should be noted that many conductive materials exhibit a reversal trend [74–76]. The powder is mixed with the dielectric liquid in the working tank. The literature describes two powder-mixed dielectric fluid circulating systems: closed and open. The working reservoir with this suspension can be isolated from the dielectric fluid circulation system in a closed system. In an open system, a powder-mixed dielectric fluid circulates continuously [73].

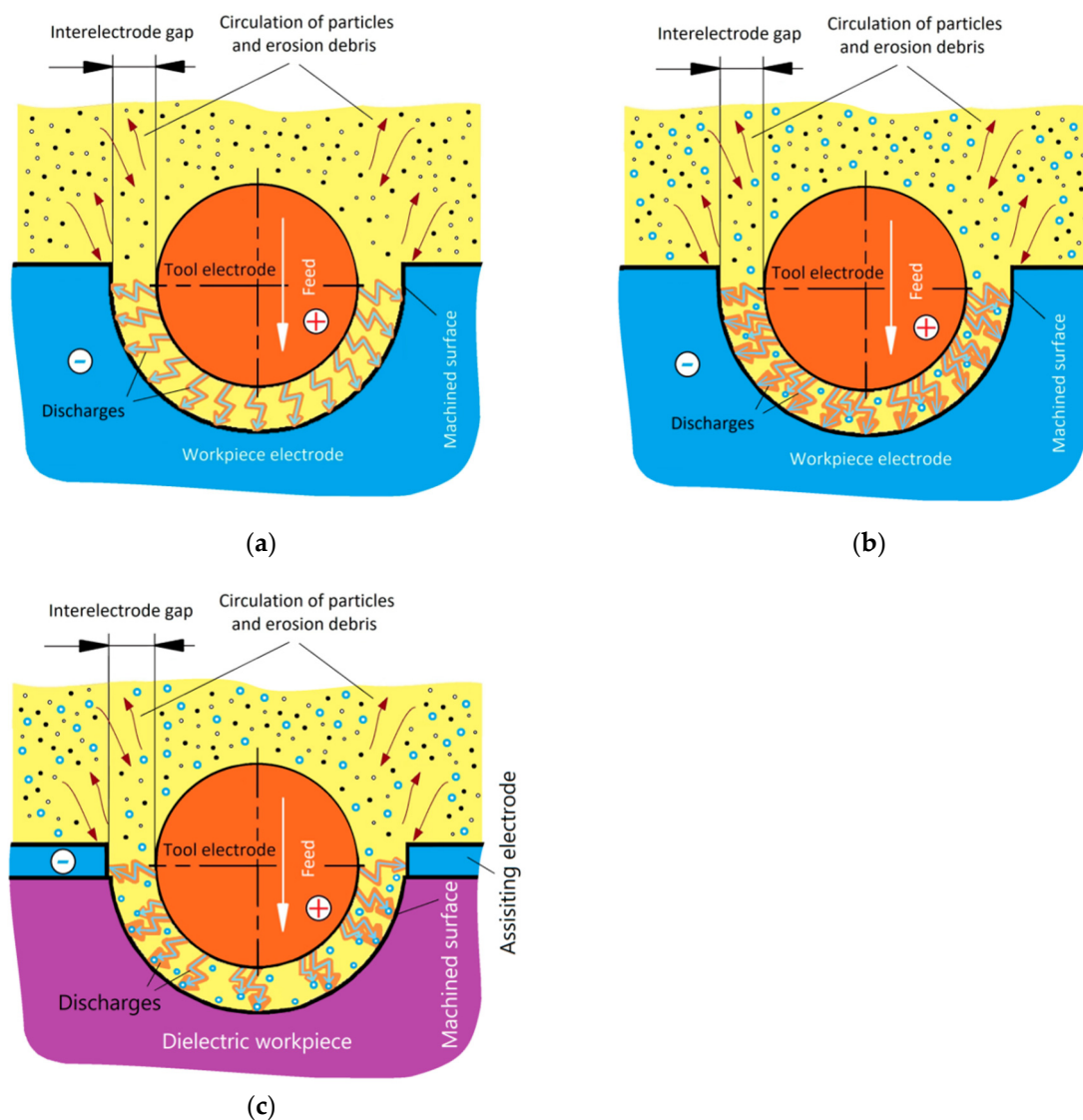


Figure 2. (a) Scheme of conventional electrical discharge machining of conductive materials; (b) scheme of powder-mixed electric discharge machining of conductive materials; (c) developed scheme of electric discharge machining of insulating materials using assisting electrode technique (combined approach).

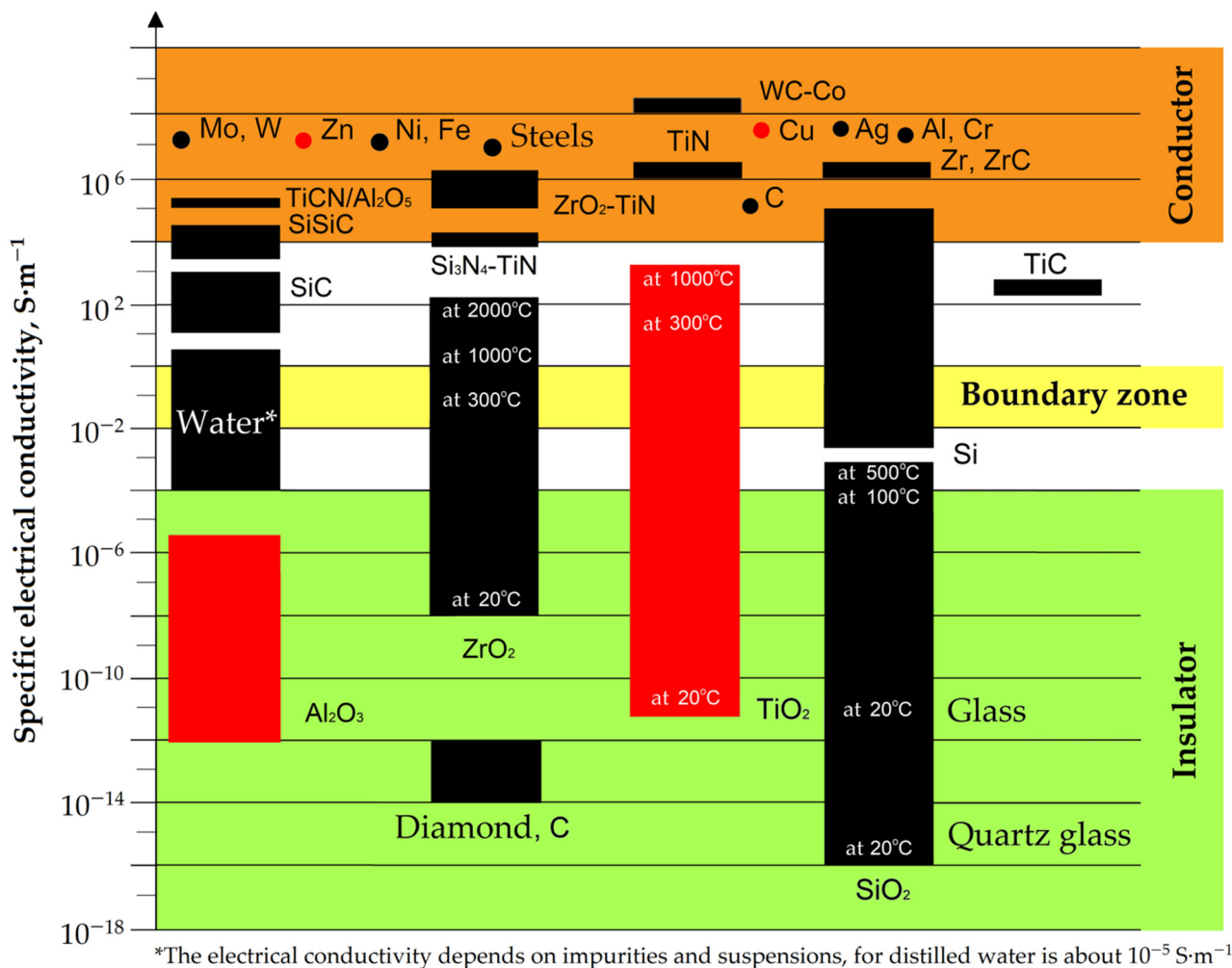


Figure 3. Specific electrical conductivity of some substances: the field of limit values for conductive materials is marked orange; for insulating materials, it is marked green; the boundary zone is marked yellow; the materials chosen for the current research are marked red.

The present study used a closed system where current discharges were addressed to the introduced micro-sized particles, uniformly suspended in the volume of the dielectric medium (suspension) in the interelectrode gap. TiO_2 material was chosen for assisting powder due to the following reasons:

- It is commercially available and relatively safe for the personnel when working with micro-sized particles in suspension (health hazard code 1: exposure may cause only irritation with minimal residual damage, according to NFPA 704), toxic in the form of nanoparticles;
- Insoluble in water;
- Exhibits increased electrical conductivity to a level close to the one for conductive materials in the presence of heat (more than 1000°C) (Figure 3);
- Exhibits semiconductive properties at normal temperatures (*n*-type with the band gap $E_g = 3.0 \text{ eV}$ for rutile, $E_g = 3.20 \text{ eV}$ for anatase [77]; the less the band gap is, the more conductive properties exhibit material [78,79]);
- Transforms into rutile form when heated.

The purpose of the study is to increase the productivity of electrical discharge machining of alumina using assisting means such as conducting coating powder-mixed dielectric medium based on water. The performance is evaluated by calculating the volumetric

material removal rate varying pulse frequency and powder concentration. The results of the current study are compared with the closest analogs.

The scientific novelty consists of establishing stable relationships between machining performance using the assisting electrode technique and the experimental factors, the electrical properties of the assisting materials, and developing an alternative approach in micro texturing cutting ceramics.

2. Materials and Methods

2.1. Sintering of the Samples

The corundum α -Al₂O₃ A16SG (Alcoa, New York, NY, USA) was used for producing samples. The average particle diameter was 0.53 μ m. Granulometric analysis of powder was carried out on an optical granulomorphometer 500NANO (Occhio, Liege, Belgium). Powder mixtures were prepared and ground in a Turbula multidirectional shaker (Eskens B.V., Alpen aan den Rijn, The Netherlands) in ethanol in a polyethylene container at 150 rpm for 24 h. Suspensions were dried in a FreeZone2.5 lyophilizer (LabConco, Kansas, MO, USA) at -50 ± 2 °C, while the sheath temperature was $+23 \pm 2$ °C. During the entire processing, the pressure in the chamber was 0.02 ± 0.01 mbar [80]. The powder mixtures were freely poured into mechanically produced graphite molds [81] fabricated of MPG-6 grade cold-pressed blanks of 1 μ m-sized powder particles. Graphite molds machining was carried out on a CTX beta 1250 TC turning and milling machine (DMG MORI, Bielefeld, Germany) with a roughing spindle speed of 100–300 m/min, feed of 0.1 mm/tooth, finishing speed of 150–600 m/min, feed of 0.013–0.05 m/min, by a carbide tool with a multi-layer combined PVD-coating [82,83]. Machining was accompanied by parameter control using a diagnostic system (MSUT Stankin, Moscow, Russia) [84–86]. The powder mixture was sintered in a graphite mold on a spark plasma sintering machine KCE FCT-H HP D-25 SD (FCT Systeme GmbH, Rauenstein, Germany) at 1400 °C with a heating rate of 100 °C min⁻¹ at uniaxial pressure 80 MPa in vacuum for 10 min [48,87–89]. The sintered discs were 65.5 mm in diameter and 10 mm in thickness.

Optical control was carried out on an Olympus BX51M instrument (Ryf AG, Grenchen, Switzerland). Scanning electron microscopy of mechanically produced fracture and chemical analyses were conducted on a VEGA3 instrument (Tescan, Brno, Czech Republic). Sample density measurements were carried out in distilled water (ceramic samples were boiled for 5 h and then soaked for 24 h) using the Archimedes principle and compared with theoretical values (3.89 g/cm³ for Al₂O₃). X-ray diffraction analysis of the samples was conducted on an Empyrean diffractometer (PANalytical, the Netherlands) using a tube with a copper anode. The cross sections of the samples were prepared on ATM Machine Tools (ATM Machine Tools Ltd., Wokingham, UK).

2.2. Electrical Discharge Machining

A two-axis wire electrical discharge machine ARTA 123 Pro (NPK “Delta-Test”, Fryazino, Moscow Oblast, Russia) was used for experiments (Table 1). The open tank system of the machine allows using any possible dielectric medium (deionized water, mineral oil, water- or oil-based suspensions) out of the filtration system.

Table 1. Main characteristics of wire electrical discharge machine ARTA 123 Pro.

Parameters	Value and Description
Max axis motions X × Y × Z, mm	125 × 200 × 80
Tool positioning accuracy, μ m	± 1
Average surface roughness parameter R_a , μ m	0.6
Dielectric medium	Any
Max power consumption, kW	<6

A brass wire electrode of 0.25 mm in diameter fabricated of CuZn35 brass provided texture formation on alumina without taking into account the spark gap (path offset). The

preliminary testing in water-medium reduced the range of the machining factors. The range of the chosen factors is presented in Table 2. The previously conducted work with alumina showed that the optimal value of the operational current is 15 A. During the study, it was decided to limit the research area to EDM factors such as pulse frequency, and concentration of the powder in the fluid to make it more straightforward since the main correlation between current, operational voltage, and character of the obtained wells on the surface or material removal rate is known and understandable [90]:

$$\sum F_{imp} = I \cdot V_O \quad (1)$$

where $\sum F_{imp}$ is the summarized force of working impulses in the system's action, N; I is current, A; and V_O is operational voltage, V.

Table 2. Range of electrical discharge machining factors.

Factor	Measuring Units	Value
Operational voltage, V_O	V	108
Pulse frequency, f	kHz	2; 5; 8; 11
Pulse duration, D	μ s	1
Rewinding speed, v_W	m/min	7
Feed rate, v_F	mm/min	0.3
Wire tension F_T	N	0.25

Machining is carried out according to the control program of the translational movement of the wire electrode along the X-axis from the zero position to a depth of 0.98 mm (taking into account the spark gap) [91–93].

The development of factors was carried out following the results of pre-implemented experiments. The factors depended on the machine's capabilities and were limited by the results of each experiment. Each failed experiment minimized the range of the factors and assisted in determining the optimal values in terms of the material removal rate (productivity) [94].

The coated blank was fixed on the machine table during experiments, ensuring immobility. The basing was carried out by wire tool approach along the X- and Y-axes; the surface of the coated workpiece was taken as zero. Before the start of processing, a spark adjusted the wire electrode vertically along the Z-axis. The position from +2 to +3 mm from the surface of the assisting coating was taken as the initial position of the wire electrode. The nozzles of the working fluid are brought as close as possible to the coated blank after the wire electrode location to ensure adequate flushing of the working area. The nozzles from which the dielectric is supplied are located on two sides of the coated blank, directing the jet into the interelectrode gap between the coated blank and wire electrode to ensure its turbulent character. Processing is carried out with complete immersion in the dielectric. When the workpiece is immersed, the dielectric level is provided above the workpiece (blank) level by 1–2 mm. Before machining, the workpiece was held for 8–10 min in a dielectric to avoid the influence of thermal fluctuations due to the difference in ambient temperatures, electrodes, workpiece, and the dielectric fluid. At the end of the electrical discharge machining, the blank was taken out from the tank. The resulting sample was wiped with a rag in place. Formed textures (kerfs) were controlled optically. The scheme of coated blank fixing on the equipment is shown in [95].

The parameters of the kerf were controlled by optical microscopy. Here and below, the optical measurement error was calculated by the formula [96–99]:

$$\delta_l = \pm 3 + \frac{L}{30} + \frac{g \cdot L}{4000}, \quad (2)$$

$$\delta_t = \pm 3 + \frac{L}{50} + \frac{g \cdot L}{2500}, \quad (3)$$

where δ_l is the longitudinal measurement error, μm ; δ_t is the transversal measurement error, μm ; L is the measured length, mm ; and g is the product height above microscope table glass (taken equal to zero), mm .

The volumetric material removal rate (MRR) was calculated through the feed rate of the wire electrode into the working area and the volume of removed material (Figure 4) [100]:

$$S = \frac{1}{2} r'_w{}^2 (\alpha - \sin \alpha) \quad (4)$$

where S is the kerf area in the plan, mm^2 ; r'_w is the radius of the electrode tool taking into account the spark gap ($r_w + \Delta$), mm ; and α is the angle of the formed segment in the plan, rad :

$$\alpha = 2 \cdot \arccos \left(\frac{r'_w - h}{r'_w} \right), \quad (5)$$

where h is the depth of the kerf, μm . The radius of the electrode tool taking into account the spark gap r'_w is calculated as follows:

$$r'_w = r_w + \Delta, \quad (6)$$

where r_w is the wire electrode radius ($125 \mu\text{m}$), μm ; the spark gap Δ was taken as $48 \pm 9.6 \mu\text{m}$ for the materials with the threshold conductivity from the previously conducted studies [39,90,91,101].

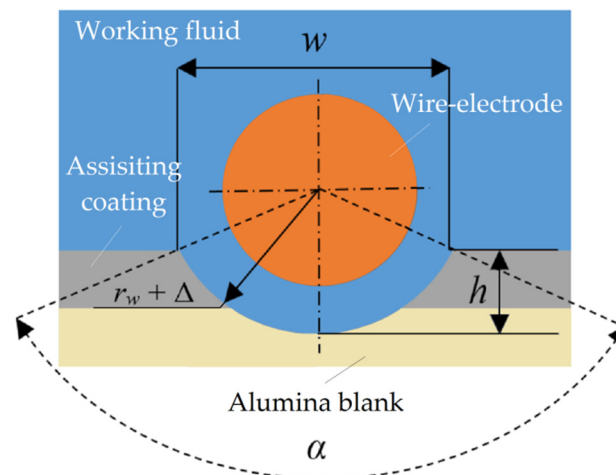


Figure 4. Scheme for calculating the cut area of the formed kerf during electrical discharge machining using assisting electrode technique.

The volume of removed material is calculated using the formula [90]:

$$V = S \cdot l \quad (7)$$

where l is the length of the kerf, μm , then the material removal rate is:

$$MRR = \frac{V}{t} \quad (8)$$

where t is the processing time calculated from the feed rate v_F of the electrode tool, s :

$$t(\text{s}) = \frac{h(\text{mm})}{v_F \left(\frac{\text{mm}}{\text{s}} \right)} \quad (9)$$

2.3. Assisting Suspension

Deionized water (LLC "Atlant", pos. Marusino, Lyubertsy district, Moscow region, The Russian Federation) following ASTM D-5127-90 with specific electrical resistivity

up to 18.0 MΩ·cm was chosen as a suspension basis to avoid formation insulating and explosive debris that may hamper electrical discharge machining and may have dramatic consequence in terms of safety (formation of Al₄C₃ or Al₂(C₂)₃) [68–70].

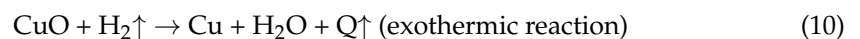
Water-based suspension of TiO₂ with various concentrations (50, 100, 150 g/L) was used as a dielectric medium. The following powder was used for producing suspension:

- Titanium(IV) oxide TiOx-271 grade (LLC “Titanium Investments”, Armyansk, Republic of Crimea, The Russian Federation), following GOST 9808-84, with an average particle diameter $d_{50} = 9.29\text{--}13.94\ \mu\text{m}$.

The powder was subjected to granulometric analysis and optical microscopy. An EL104 (Mettler Toledo, Columbus, OH, USA) laboratory balance with a measurement range of 0.0001–120 g weighed the powder with an error of 0.0001 g in preparing the suspension. Initial TiO₂ powder was sifted using an analytical sieving machine AS200 basic (Retsch, Dusseldorf, Germany) with a test sieve (10 μm by ISO 3310-1). It should be noted that the smallest size of suspended particles led to the highest rate of volumetric material removal and the lowest wear of the primary tool electrode [102–106]. Another reason for using 10 μm granules is the narrow range of the discharge gap: for the conductive materials, it is about 170–200 μm [90,95]; for materials with the threshold conductivity, it is 48–50 μm [49,80,91]. In this case, the electrical conductivity and the discharge gap are in direct proportion [101]. The prepared suspension was constantly stirred during experiments. After processing, the samples were cleaned with alkali.

2.4. Assisting Electrode

The most typical coating for the assisting electrode technique used in the works of many authors is copper foil or sheet placed adhesively on the surface of the ceramic blank [51,65,107,108]. Copper and copper group metals and alloys based on them form insulating oxides that are unstable in the presence of hydrogen of medium (in the case of Cu, reduction to metallic copper) [109–113]:



or dissociates at temperatures above 280 °C for Ag₂O, above 100 °C for Ag₂O₂, and above 225 °C for Au₂O, when Au₂O₃ is stable and exhibits conductive properties [114,115]. This property of copper (II) oxide, combined with its inertness to the media and other components of the working area, makes copper unrepeatable when designing technology for a wide group of materials.

A HomaFix 404 (20 m × 10 mm) copper tape (JSC Electroma, Lipetsk, Russia) was used as an assisting coating. The main properties of the tape are provided in Table 3. The specific electrical resistance of the assisting coating (Table 4) was controlled by a Fischer Sigmascop SMP10 device (Helmut Fischer GmbH, Sindelfingen, Germany) by evaluating the electric conductance at normal temperature in Siemens and the percentage of the electrical conductance of the control sample fabricated of annealed bronze in the range of 1–112%.

Table 3. Parameters of copper tape.

Parameter	Value
Thickness of copper basis, mm	0.035 ± 0.0002
Tensile strength, N/cm	115
Elongation (Extension ratio), %	<2
Specific electrical resistivity, Ω·mm ² ·m ^{−1}	0.016–0.017
Operating temperature, °C	from −40 to +110 with a tolerance of ±5
Tape width, mm	10

Table 4. Electrical properties of some substances.

Assisting Coating	Electrical Conductivity ¹ , Sm·cm ⁻¹	Specific Electrical Resistivity ² , Ω·mm ² ·m ⁻¹
Copper tape, resin-based adhesive	0.580046 ± 0.00001	0.01724 × 10 ⁻⁶
Graphite ³	-	8.00
Distilled water ³	-	10 ³ ÷ 10 ⁴

¹ Experimental values; ² calculated values; ³ for reference.

Before coating, the ceramic samples were placed in an ultrasonic tank and cleaned using a soap solution at a temperature of 60 °C for 20 min and alcohol for 5 min [116]. Approbation of the coated samples was conducted in a deionized water medium. Coating removal was conducted by a complex method: washing in an ultrasonic tank and mechanical cleaning.

3. Results

3.1. Characterization of Al₂O₃ Samples

A microphotograph of Al₂O₃ powder is presented in Figure 5a. It shows a predominantly favorable spherical shape of particles that contributes to reducing the porosity of the samples. The variety of particle sizes has a positive effect on the mechanical properties of the samples.

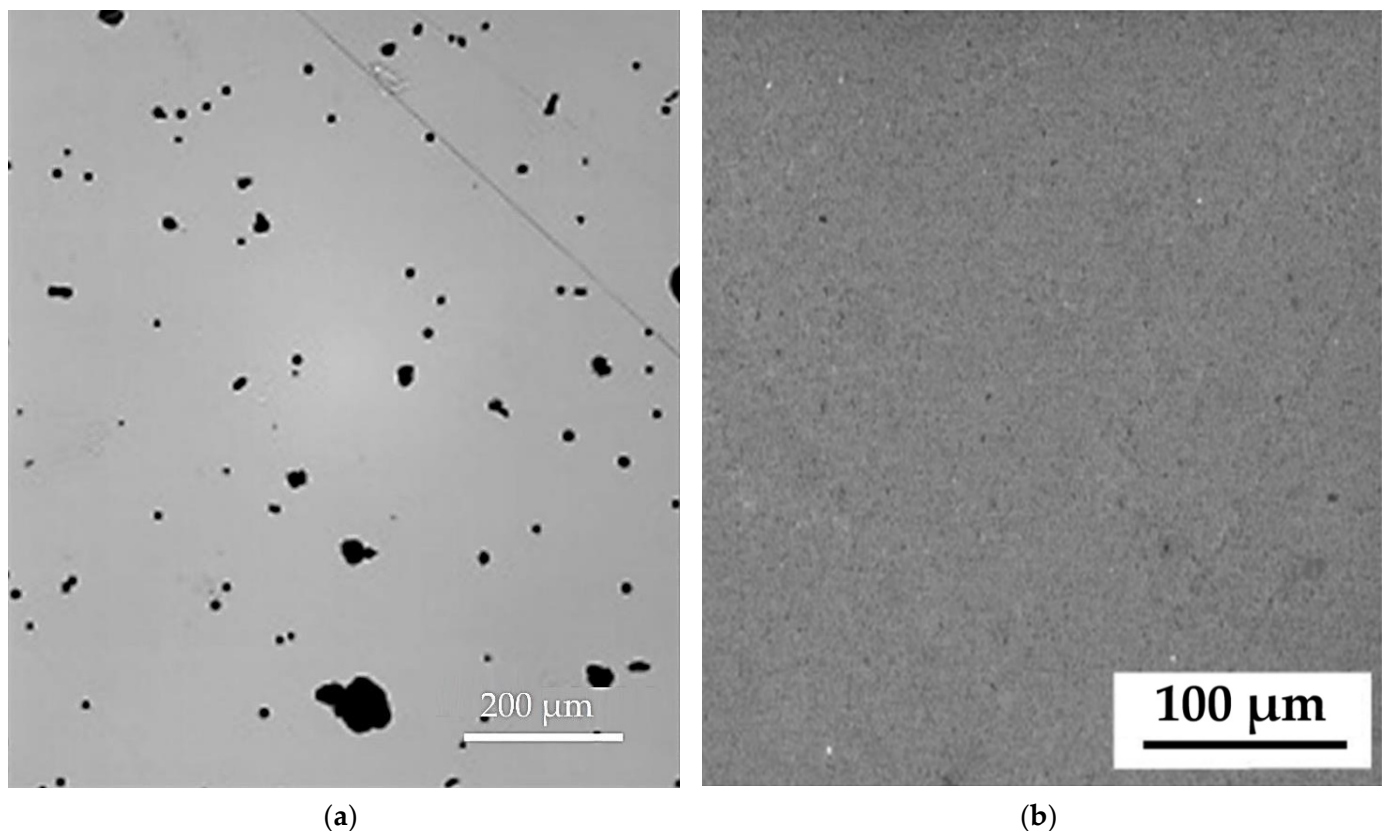


Figure 5. (a) Morphology of Al₂O₃ powder; (b) polished surface of the sintered sample (SEM image).

The polished surface of the sintered sample is presented in Figure 5b. The density of the samples after sintering was 99.2 ± 0.2%. X-ray diffraction analyses did not reveal any contamination by other phases nor traces of any side reactions during sintering. The chemical analysis of the samples at the fracture site corresponds to the theoretical chemical composition of the ceramics.

3.2. Characterization of TiO₂ Powder

Granulometric analysis (Figure 6a, Table 5) of TiO₂ powder showed that the powder sample had an average inner diameter of 10.84 μm and 9.29 μm for 50% of the particles, while the average area diameter was 16.12 μm and 13.94 for 50% particles. The average circularity of the titanium dioxide powder is about 0.656 μm and about 0.700 μm for 50% of the particles. Titanium dioxide granules have a specific character. Optical microscopy of the granules is shown in Figure 6b. The powder was sieved before further processing.

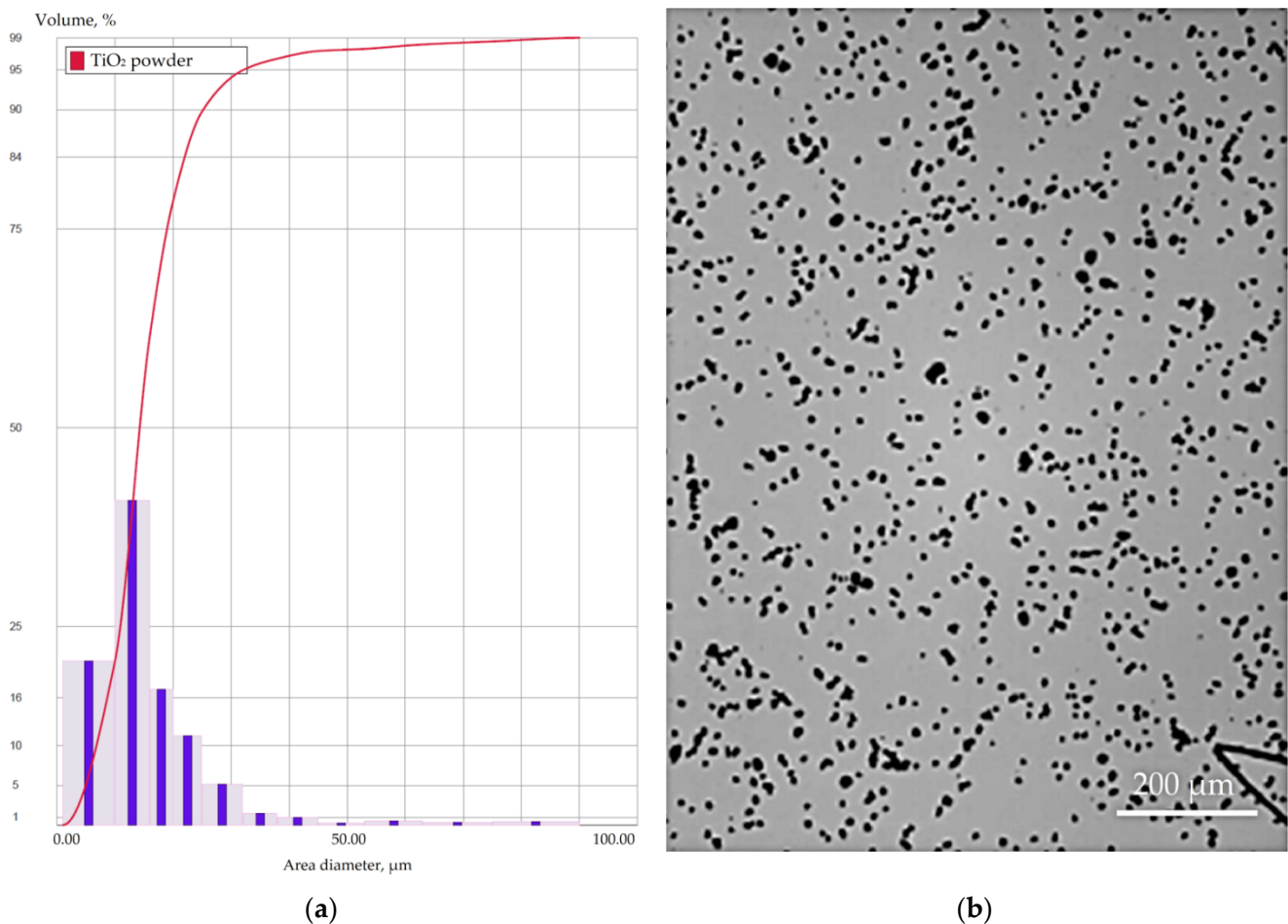


Figure 6. Granulometric analysis of the composition of titanium dioxide powder (a) and morphology (b).

Table 5. Granulometry of titanium dioxide powder.

Inner Diameter Range, μm	Volume, %	Cumulative Volume, %
1.00–10.00	20.82	20.82
10.00–16.00	41.22	62.04
16.00–20.00	17.25	79.29
20.00–25.00	11.36	90.65
25.00–32.00	5.23	95.88
32.00–38.00	1.48	97.36
38.00–45.00	0.97	98.33
45.00–53.00	0.27	98.60
53.00–63.00	0.56	99.15
63.00–75.00	0.39	99.54
75.00–90.00	0.46	100.00

3.3. Electrical Discharge Machining in TiO_2 Powder-Mixed Water Medium

The general view of the working area and results of the optical microscopy for the machined kerf for the various powder concentration and pulse frequencies are shown in Figure 7. Due to the visual optical whiteness of the ceramic material, the formed texture (kerf) is not distinguishable; however, traces of adsorbed copper and deposited drops are clearly visible and cannot be removed mechanically with effort. The deepest kerf in Al_2O_3 sintered blank using TiO_2 powder-mixed water medium was obtained for a concentration of 150 g/L, and pulse frequency $f = 2$ kHz and $f = 5$ kHz.

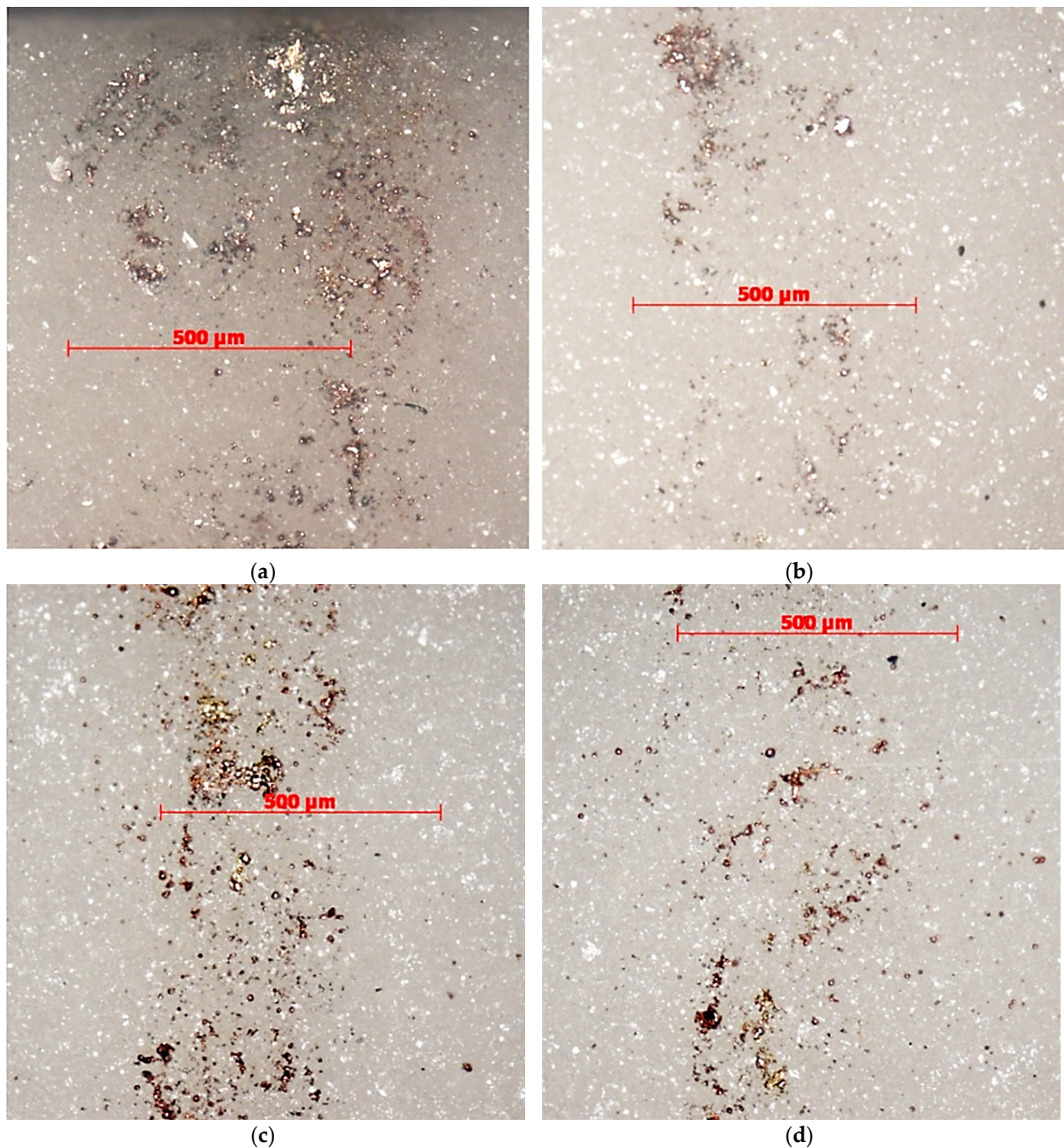


Figure 7. Optical microscopy of the obtained kerf in Al_2O_3 samples coated with a copper tape coating (general view): (a) concentration of 50 g/L, pulse frequency $f = 11$ kHz; (b) concentration of 100 g/L, pulse frequency $f = 5$ kHz; (c) concentration of 150 g/L, pulse frequency $f = 2$ kHz; (d) concentration of 150 g/L, pulse frequency $f = 7$ kHz.

3.4. Scanning Electron Microscopy (Chemical Analyses)

The results of quantitative and qualitative analysis of the obtained kerfs after electrical discharge machining of alumina using a monolayer copper tape coating are shown in Figure 8 and Table 6. The images show a uniform distribution of chemical elements such as aluminum and oxygen (Figure 8a,b) and the assisting electrode coating of copper deposited on the surface (Figure 8c). When using a suspension, the amount of deposited copper increases many times (by 81.1%) (Figure 8f, Table 6), while zinc (2.6%) of the wire tool and titanium (1.5%) of the powder are also presented (Table 6). The presence of carbon corresponds to normal atmospheric contamination of the samples.

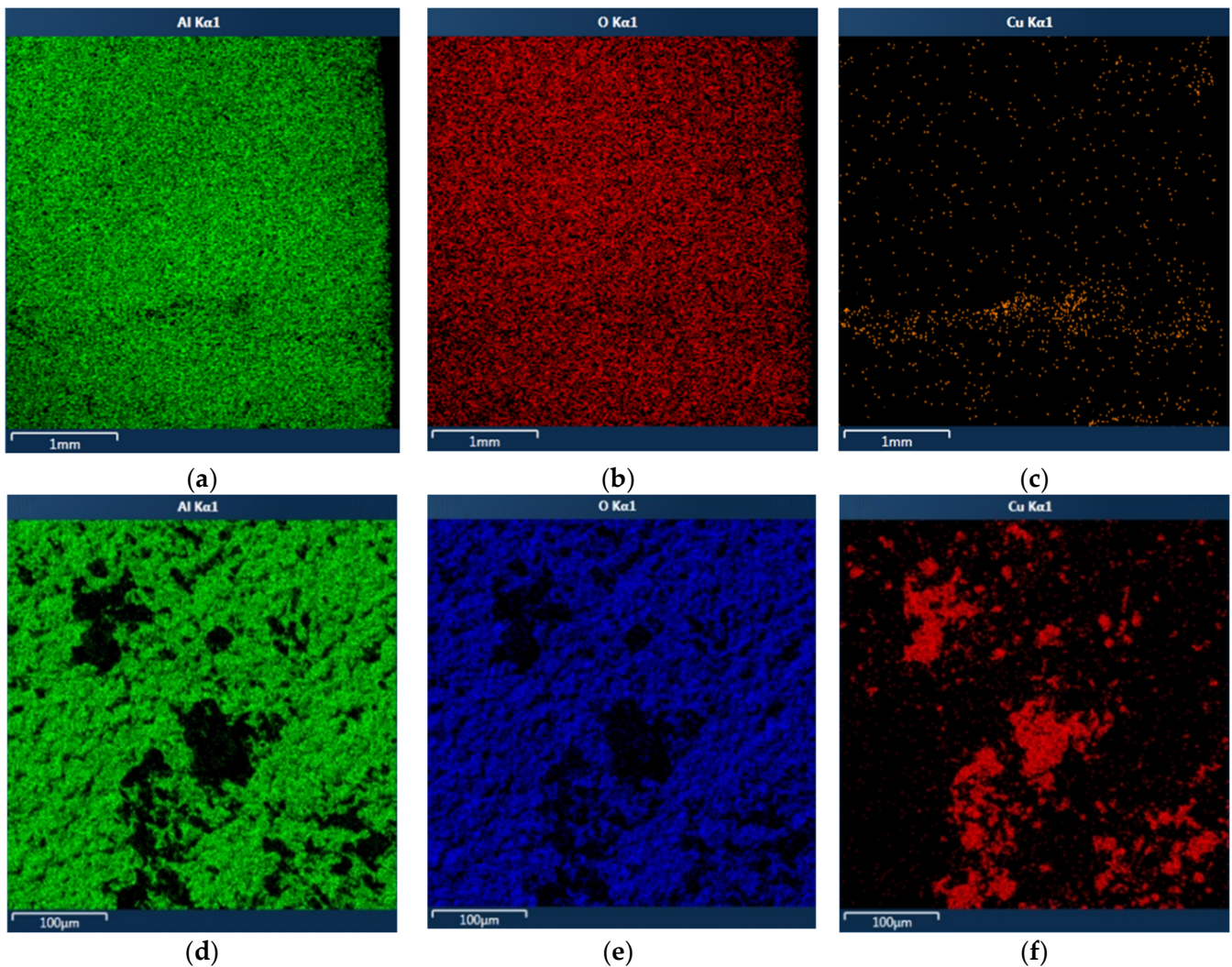


Figure 8. Chemical mapping of the machined kerf in the Al_2O_3 sample: (a) in water medium, aluminum; (b) in water medium, oxygen; (c) in water medium, copper; (d) in TiO_2 powder-mixed water medium (150 g/L), pulse frequency $f = 2$ kHz, aluminum; (e) in TiO_2 powder-mixed water medium (150 g/L), pulse frequency $f = 2$ kHz, oxygen; (f) in TiO_2 powder-mixed water medium (150 g/L), pulse frequency $f = 2$ kHz, copper.

Table 6. Chemical analysis of the machined kerf at the place of the deposited copper (average of three spectra).

Chemical Elements, wt %					
Al	O	Cu	Zn	Ti	C
0.5	6.0	81.1	2.6	1.5	8.3

3.5. Material Removal Rate

An analysis of the processing performance of alumina using the combined approach of assisting electrode techniques was carried out for TiO₂ concentration of 50, 100, and 150 g/L in a water medium for the pulse frequency (f) range of 2–11 kHz. The measured values of the kerf parameters and the calculated values of the machined segment angle are shown in Table 7. The material removal rate is shown in Table 8. A graphical presentation of the relationship between material removal rate, pulse frequency, and TiO₂ concentration is shown in Figure 9. The higher performance was achieved for pulse frequencies 2 and 5 kHz and a concentration of 150 g/L.

Table 7. The kerf parameters and calculated angle of the segment in plan α of the machined alumina using a copper tape coating and TiO₂ powder-mixed water medium.

TiO ₂ Con- centration, g/L	Pulse Frequency f , kHz	Kerf Depth h , μm	Kerf Width w , μm	Kerf Length l , μm	Angle of Segment in Plan α , Rad
50	2	26.75	155.93	2950.00	0.56
	5	33.27	155.93	1600.00	0.62
	8	26.53	140.03	2000.00	0.56
	11	23.93	129.55	3000.00	0.53
100	2	51.50	149.19	5550.00	0.78
	5	37.52	143.07	5100.00	0.67
	8	22.87	124.38	5550.00	0.50
	11	36.91	140.40	3800.00	0.66
150	2	56.70	181.70	6750.00	0.83
	5	51.61	111.46	7250.00	0.79
	8	33.17	138.13	5000.00	0.63
	11	36.64	145.89	7000.00	0.59

Table 8. The material removal rate of electrical discharge machining alumina ceramics using a copper tape coating and TiO₂ powder-mixed water medium.

TiO ₂ Con- centration, g/L	Pulse Frequency f , kHz	Kerf Area in Plan S , mm^2	Volume of Removed Material V , mm^3	Estimated Machining Time t , s	Volumetric Material Removal Rate, mm^3/s
50	2	0.00044	0.00130	5.35	0.00024
	5	0.00059	0.00094	6.65	0.00014
	8	0.00043	0.00087	5.31	0.00016
	11	0.00037	0.00111	4.79	0.00023
100	2	0.00116	0.00646	10.30	0.00063
	5	0.00073	0.00373	7.50	0.00050
	8	0.00031	0.00172	4.57	0.00038
	11	0.00070	0.00265	7.38	0.00036
150	2	0.00140	0.00942	11.34	0.00083
	5	0.00120	0.00870	10.32	0.00084
	8	0.00061	0.00304	6.63	0.00046
	11	0.00049	0.00344	7.33	0.00047

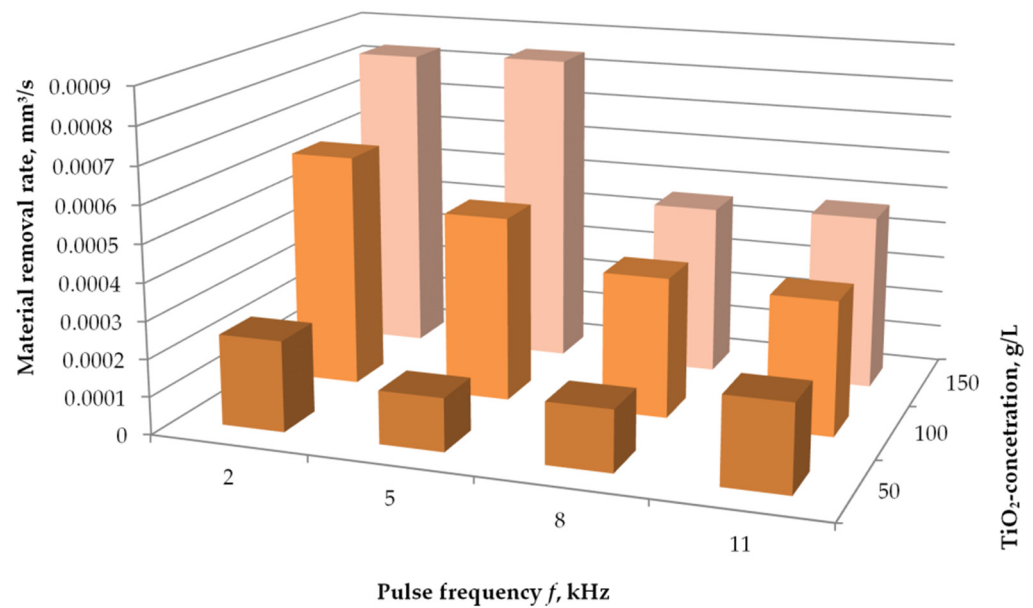


Figure 9. The performance of electrical discharge machining of alumina using a copper tape coating and TiO₂ powder-mixed water medium.

4. Discussion

A comparison of the performance of electrical discharge machining alumina was carried out for the current study's data and previously published (Table 9). The present results were compared with those obtained with a brass electrode tool in a water-based medium and those obtained using hydrocarbons. The data indicate that the developed method is superior to:

- The previously developed technique of electrical discharge machining using a brass electrode tool in water-based working fluid [80] and;
- The published data on electrical discharge machining alumina in hydrocarbons using monolayer copper foil of 6 μm in thickness [65].

Table 9. Comparison of performance parameter of electrical discharge machining alumina based on the use of assistive tools.

Primary Electrode Tool	Assisting Electrode Coating	Assisting Suspension	Working Fluid	Material Removal Rate, mm ³ /s	Reference
Brass wire, $\text{\O}0.25$ mm	Copper tape, 40 μm	TiO ₂ particles, $\text{\O}10$ μm , 150 g/L	Deionized water	0.0084	Current study
Brass wire, $\text{\O}0.25$ mm	Ni-Cr PVD coating, 12 μm	SnO particles, $\text{\O}10$ μm , 150 g/L	Deionized water	0.0014	[80]
Copper prism, 5 \times 5 mm	Copper foil, 6 μm	-	Mineral oil (hydrocarbons)	0.0051	[65]
Copper tube, $\text{\O}3.5$ mm (inner— $\text{\O}3.0$)	Resin-based carbon tape	Graphite particles, $\text{\O}30$ μm , 7–10 g/L	Kerosene (hydrocarbons)	0.0213	[66]

The results published for the technique using carbon tape [66] exceed the values of the present study but demonstrate significant shortcomings typical for sinker type of machining and working with carbons and hydrocarbons:

- The manufacture of a unique electrode is required;
- There is no possibility of processing ruled surfaces;
- Graphite particles exhibit electrical anisotropy (electrical properties are different in different directions of the crystal lattice) [117];
- It creates risks of the formation of chemically unstable dielectric carbides with all the ensuing consequences for equipment and personnel (Al_3C_4 or $\text{Al}_2(\text{C}_2)_3$) [44,68–70].

The relationship between productivity and electrical properties of coatings and assisting powders is shown in Figure 10. The study [65] was not considered due to the measured data absence for the electrical resistance/conductivity of the developed coating and the absence of the assisting powder used in the study. For [66], the available data for the graphite were taken into consideration. The specific electrical conductivity is provided in Table 4. The band gap (E_g) was taken as an average value of 0.4–1.0 eV [118–120].

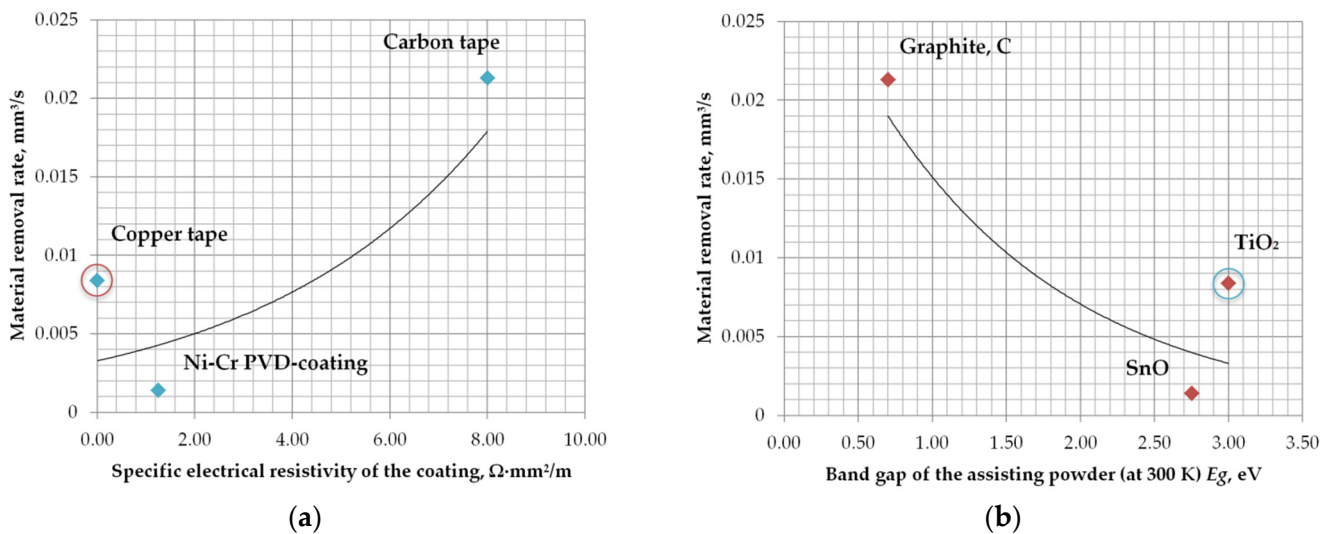


Figure 10. Relationships between the productivity of the electrical discharge machining of alumina and the electrical properties of the assisting materials: (a) specific electrical resistivity of coatings; (b) band gap of assisting powders.

5. Conclusions

The paper solves a scientific and technical problem relevant to modern mechanical engineering and metalworking, which consists of increasing the productivity of electrical discharge machining of dielectric material, alumina, using the combined approach using assisting copper tape coating of 40 μm and TiO_2 powder-mixed dielectric medium. Using TiO_2 powder-mixed water-based dielectric medium was proposed for the first time. The choice of water as a dielectric basis is substantiated by the safety of the personnel and equipment since the dissociation of hydrocarbons creates risks of the formation of chemically unstable dielectric carbides (methanide Al_3C_4 and acetylenide $\text{Al}_2(\text{C}_2)_3$). The choice of the powder is substantiated by the electrical properties of titanium dioxide.

The conducted work allowed us to establish relationships between the performance of the machining Al_2O_3 ceramics and experimental factors such as pulse frequency and powder concentration. The highest values for the productivity of 0.0083–0.0084 mm^3/s were achieved for pulse frequency 2 kHz and 5 kHz and TiO_2 powder concentration of 150 g/L. This exceeds the analog for copper tape coating by 1.64 times and has the advantage of not using hydrocarbons.

The comparison of the performance (0.0083–0.0084 mm^3/s) with the performance of the analogs shows that the results may correlate with the electrical properties of the assisting materials: the electrical resistance of the deposited coating and the band gap of the used powder. However, it requires further research.

The complex works proved the combined approach's effectiveness in texturing alumina to a depth of up to $54.16 \pm 0.05 \mu\text{m}$ with a thickness of the blank of up to 5.00 mm using a brass wire with a diameter of 0.25 mm.

On the basis of the obtained theoretical and experimental research results and the production experience, the developed method can be applied to texturing cutting plates fabricated of cutting ceramics.

Author Contributions: Conceptualization, S.N.G.; methodology, M.A.V.; software, A.S.M.; validation, K.H.; formal analysis, A.S.M.; investigation, A.S.M., and S.N.G.; resources, M.A.V.; data curation, K.H.; writing—original draft preparation, A.A.O.; writing—review and editing, A.A.O.; visualization, K.H. and A.A.O.; supervision, S.N.G.; project administration, M.A.V.; funding acquisition, S.N.G. All authors have read and agreed to the published version of the manuscript.

Funding: This work is funded by the state assignment of the Ministry of Science and Higher Education of the Russian Federation, Project No. FSFS-2021-0003.

Data Availability Statement: Data are available in a publicly accessible repository.

Acknowledgments: The study was carried out on the equipment of the center of collective use of MSUT "STANKIN" supported by the Ministry of Higher Education of the Russian Federation (project No. 075-15-2021-695 from 26.07.2021, unique identifier RF-2296.61321X0013).

Conflicts of Interest: The authors declare no conflict of interest.

References

1. Grigoriev, S.N.; Volosova, M.A.; Fedorov, S.V.; Okunkova, A.A.; Pivkin, P.M.; Peretyagin, P.Y.; Ershov, A. Development of DLC-Coated Solid SiAlON/TiN Ceramic End Mills for Nickel Alloy Machining: Problems and Prospects. *Coatings* **2021**, *11*, 532. [\[CrossRef\]](#)
2. Kuzin, V.; Grigoriev, S.N.; Volosova, M.A. The role of the thermal factor in the wear mechanism of ceramic tools: Part 1. Macrolevel. *J. Frict. Wear* **2014**, *35*, 505–510. [\[CrossRef\]](#)
3. Oppong Boakye, G.; Geambazu, L.E.; Ormsdottir, A.M.; Gunnarsson, B.G.; Csaki, I.; Fanicchia, F.; Kovalov, D.; Karlsdottir, S.N. Microstructural Properties and Wear Resistance of Fe-Cr-Co-Ni-Mo-Based High Entropy Alloy Coatings Deposited with Different Coating Techniques. *Appl. Sci.* **2022**, *12*, 3156. [\[CrossRef\]](#)
4. Mahesh, K.; Philip, J.T.; Joshi, S.N.; Kuriachen, B. Machinability of Inconel 718: A critical review on the impact of cutting temperatures. *Mater. Manuf. Process.* **2021**, *36*, 753–791. [\[CrossRef\]](#)
5. Stepanov, N.D.; Shaysultanov, D.G.; Chernichenko, R.S.; Tikhonovsky, M.A.; Zherebtsov, S.V. Effect of Al on structure and mechanical properties of Fe-Mn-Cr-Ni-Al non-equiatomic high entropy alloys with high Fe content. *J. Alloy. Compd.* **2019**, *770*, 194–203. [\[CrossRef\]](#)
6. Padalko, A.G.; Ellert, O.G.; Efimov, N.N.; Novotortsev, V.M.; Talanova, G.V.; Zubarev, G.I.; Fedotov, V.T.; Suchkov, A.N.; Solntsev, K.A. High-pressure phase transformations, microstructure, and magnetic properties of the hypereutectic alloy 10Ni-90Al. *Inorg. Mater.* **2013**, *49*, 1098–1105. [\[CrossRef\]](#)
7. Stepanov, N.D.; Shaysultanov, D.G.; Tikhonovsky, M.A.; Zherebtsov, S.V. Structure and high temperature mechanical properties of novel non-equiatomic Fe-(Co, Mn)-Cr-Ni-Al-(Ti) high entropy alloys. *Intermetallics* **2018**, *102*, 140–151. [\[CrossRef\]](#)
8. Zhong, Q.; Wei, K.; Yue, X.; Zhou, R.; Zeng, X. Powder densification behavior and microstructure formation mechanism of W-Ni alloy processed by selective laser melting. *J. Alloy. Compd.* **2022**, *908*, 164609. [\[CrossRef\]](#)
9. Pingale, A.D.; Belgamwar, S.U.; Rathore, J.S. A novel approach for facile synthesis of Cu-Ni/GNPs composites with excellent mechanical and tribological properties. *Mater. Sci. Eng. B Solid-State Mater. Adv. Technol.* **2020**, *260*, 114643. [\[CrossRef\]](#)
10. Mohsan, A.U.H.; Liu, Z.; Padhy, G.K. A review on the progress towards improvement in surface integrity of Inconel 718 under high pressure and flood cooling conditions. *Int. J. Adv. Manuf. Technol.* **2017**, *91*, 107–125. [\[CrossRef\]](#)
11. Filippov, A.V.; Tarasov, S.Y.; Podgornyh, O.A.; Shamarin, N.N.; Filippova, E.O. Oriented microtexturing on the surface of high-speed steel cutting tool. *AIP Conf. Proc.* **2016**, *1783*, 020057.
12. Volosova, M.A.; Grigor'ev, S.N.; Kuzin, V.V. Effect of titanium nitride coatings on stress structural inhomogeneity in oxide-carbide ceramic. Part 2. Concentrated force action. *Refract. Ind. Ceram.* **2015**, *55*, 487–491. [\[CrossRef\]](#)
13. Niketh, S.; Samuel, G.L. Surface textured drill tools—an effective approach for minimizing chip evacuation force and burr formation during high aspect ratio machining of titanium alloy. *J. Manuf. Sci. Eng. Trans. ASME* **2021**, *143*, 041005. [\[CrossRef\]](#)
14. Fedorov, S.V.; Pavlov, M.D.; Okunkova, A.A. Effect of structural and phase transformations in alloyed subsurface layer of hard-alloy tools on their wear resistance during cutting of high-temperature alloys. *J. Frict. Wear* **2013**, *34*, 190–198. [\[CrossRef\]](#)
15. Volgin, V.M.; Lyubimov, V.V.; Kabanova, T.B.; Davydov, A.D. Theoretical analysis of micro/nano electrochemical machining with ultra-short voltage pulses. *Electrochim. Acta* **2021**, *369*, 137666. [\[CrossRef\]](#)

16. Jiang, B.; Lan, S.; Ni, J.; Zhang, Z. Experimental investigation of spark generation in electrochemical discharge machining of non-conducting materials. *J. Mater. Process. Technol.* **2014**, *214*, 892–898. [[CrossRef](#)]
17. Xie, J.; Luo, M.-J.; He, J.-L.; Liu, X.-R.; Tan, T.-W. Micro-grinding of micro-groove array on tool rake surface for dry cutting of titanium alloy. *Int. J. Precis. Eng. Manuf.* **2012**, *13*, 1845–1852. [[CrossRef](#)]
18. Yusupov, Z.A. Study of Temperatures and Residual Stresses for Face Plunge-Cut Grinding of Heat-Resistant Alloys. *Russ. Aeronaut.* **2021**, *64*, 116–121. [[CrossRef](#)]
19. Zheng, G.; Lin, Y. Tribological Properties of Micro-Groove Cemented Carbide by Laser Processing. *Micromachines* **2021**, *12*, 486. [[CrossRef](#)]
20. Ferraris, S.; Warchomicka, F.; Barberi, J.; Cochis, A.; Scalia, A.C.; Spriano, S. Contact Guidance Effect and Prevention of Microfouling on a Beta Titanium Alloy Surface Structured by Electron-Beam Technology. *Nanomaterials* **2021**, *11*, 1474. [[CrossRef](#)]
21. Wu, Z.; Deng, J.; Su, C.; Luo, C.; Xia, D. Performance of the micro-texture self-lubricating and pulsating heat pipe self-cooling tools in dry cutting process. *Int. J. Refract. Met. Hard Mater.* **2014**, *45*, 238–248. [[CrossRef](#)]
22. Pakuła, D.; Staszuk, M.; Dziekońska, M.; Koźmín, P.; Čermák, A. Laser Micro-Texturing of Sintered Tool Materials Surface. *Materials* **2019**, *12*, 3152. [[CrossRef](#)] [[PubMed](#)]
23. Vanwersch, P.; Schildermans, S.; Nagarajan, B.; Van Bael, A.; Castagne, S. Three-Dimensional Modelling of Femtosecond Laser Ablation of Metals. *Lasers Manuf. Mater. Process.* **2022**, *9*, 515–531. [[CrossRef](#)]
24. Lazarenko, B.R.; Lazarenko, N.I. Electric spark machining of metals in water and electrolytes. *Surf. Eng. Appl. Electrochem.* **1980**, *1*, 5–8.
25. Lazarenko, B.R.; Duradzi, V.N.; Bryantsev, I.V. Effect of Incorporating an additional inductance on the characteristics of anode and cathode processes. *Surf. Eng. Appl. Electrochem.* **1979**, *5*, 8–13.
26. Warregh, A.S.; Md Zain, M.Z. Study and analysis of micro fin deformation due to WEDM. *AIP Conf. Proc.* **2021**, 2339, 020083.
27. Lenin, N.; Sivakumar, M.; Selvakumar, G.; Rajamani, D.; Sivalingam, V.; Gupta, M.K.; Mikolajczyk, T.; Pimenov, D.Y. Optimization of Process Control Parameters for WEDM of Al-LM25/Fly Ash/B4C Hybrid Composites Using Evolutionary Algorithms: A Comparative Study. *Metals* **2021**, *11*, 1105. [[CrossRef](#)]
28. Vereschaka, A.S.; Grigoriev, S.N.; Sotova, E.S.; Vereschaka, A.A. Improving the efficiency of the cutting tools made of mixed ceramics by applying modifying nano-scale multilayered coatings. *Adv. Mat. Res.* **2013**, 712–715, 391–394.
29. Vereschaka, A.A.; Grigoriev, S.N.; Volosova, M.A.; Batako, A.; Vereschaka, A.S.; Sitnikov, N.N.; Seleznev, A.E. Nano-scale multi-layered coatings for improved efficiency of ceramic cutting tools. *Int. J. Adv. Manuf. Technol.* **2017**, *90*, 27–43. [[CrossRef](#)]
30. Grigoriev, S.N.; Vereschaka, A.A.; Fyodorov, S.V.; Sitnikov, N.N.; Batako, A.D. Comparative analysis of cutting properties and nature of wear of carbide cutting tools with multi-layered nano-structured and gradient coatings produced by using of various deposition methods. *Int. J. Adv. Manuf. Technol.* **2017**, *90*, 3421–3435. [[CrossRef](#)]
31. Abidi, M.H.; Al-Ahmari, A.M.; Siddiquee, A.N.; Mian, S.H.; Mohammed, M.K.; Rasheed, M.S. An Investigation of the Micro-Electrical Discharge Machining of Nickel-Titanium Shape Memory Alloy Using Grey Relations Coupled with Principal Component Analysis. *Metals* **2017**, *7*, 486. [[CrossRef](#)]
32. Lazarenko, B.R.; Mikhailov, V.V.; Gitlevich, A.E.; Verkhoturov, A.D.; Anfimov, I.S. Distribution of elements in surface layers during electric spark alloying. *Surf. Eng. Appl. Electrochem.* **1977**, *3*, 28–33.
33. Ablyaz, T.R.; Shlykov, E.S.; Muratov, K.R. The Use of Electrode Tools Obtained by Selective Laser Melting to Create Textured Surfaces. *Materials* **2022**, *15*, 4885. [[CrossRef](#)] [[PubMed](#)]
34. Doreswamy, D.; Bongale, A.M.; Piekarski, M.; Bongale, A.; Kumar, S.; Pimenov, D.Y.; Giasin, K.; Nadolny, K. Optimization and Modeling of Material Removal Rate in Wire-EDM of Silicon Particle Reinforced Al6061 Composite. *Materials* **2021**, *14*, 6420. [[CrossRef](#)]
35. Gong, S.; Meng, F.; Sun, Y.; Su, Z.; Jin, L. Experimental study on fabricating ball micro end mill with spiral blades by low speed wire electrical discharge machining. *Int. J. Adv. Manuf. Technol.* **2020**, *108*, 2541–2558. [[CrossRef](#)]
36. Volosova, M.A.; Okunkova, A.A.; Povolotskiy, D.E.; Podrabinnik, P.A. Study of electrical discharge machining for the parts of nuclear industry usage. *Mech. Ind.* **2015**, *16*, 706. [[CrossRef](#)]
37. Liu, H.-D.; Xi, X.-C.; Chen, M.; Zhao, W.-S.; Chen, H. Jump Motion Planning for Shrouded Blisks Multi-Axis EDM with Short Line Segments. *Procedia CIRP* **2018**, *68*, 399–404. [[CrossRef](#)]
38. Moghanizadeh, A. Reducing side overcut in EDM process by changing electrical field between tool and work piece. *Int. J. Adv. Manuf. Technol.* **2017**, *90*, 1035–1042. [[CrossRef](#)]
39. Melnik, Y.A.; Kozochkin, M.P.; Porvatov, A.N.; Okunkova, A.A. On adaptive control for electrical discharge machining using vibroacoustic emission. *Technologies* **2018**, *6*, 96. [[CrossRef](#)]
40. Grigoriev, S.N.; Kozochkin, M.P.; Kropotkina, E.Y.; Okunkova, A.A. Study of wire tool-electrode behavior during electrical discharge machining by vibroacoustic monitoring. *Mech. Ind.* **2016**, *17*, 717. [[CrossRef](#)]
41. Mirsch, S.; Reimer, H. Preparation and electrical properties of Al—AlN—Si structures. *Phys. Status Solidi A* **1972**, *11*, 631–635. [[CrossRef](#)]
42. Uemura, Y.; Tanaka, K.; Iwata, M. Some properties of thin aluminium nitride films formed in a glow discharge. *Thin Solid Film.* **1974**, *20*, 11–16. [[CrossRef](#)]
43. Grigoriev, S.N.; Hamdy, K.; Volosova, M.A.; Okunkova, A.A.; Fedorov, S.V. Electrical Discharge Machining of Oxide and Nitride Ceramics: A Review. *Mater. Des.* **2021**, *209*, 109965. [[CrossRef](#)]

44. Volosova, M.; Okunkova, A.; Peretyagin, P.; Melnik, Y.A.; Kapustina, N. On Electrical Discharge Machining of Non-Conductive Ceramics: A Review. *Technologies* **2019**, *7*, 55. [[CrossRef](#)]
45. Grigoriev, S.; Pristinitskiy, Y.; Volosova, M.; Fedorov, S.; Okunkova, A.; Peretyagin, P.; Smirnov, A. Wire electrical discharge machining, mechanical and tribological performance of TiN reinforced multiscale SiAlON ceramic composites fabricated by spark plasma sintering. *Appl. Sci.* **2021**, *11*, 657. [[CrossRef](#)]
46. Rashid, A.; Bilal, A.; Liu, C.; Jahan, M.P.; Talamona, D.; Perveen, A. Effect of Conductive Coatings on Micro-Electro-Discharge Machinability of Aluminum Nitride Ceramic Using On-Machine-Fabricated Microelectrodes. *Materials* **2019**, *12*, 3316. [[CrossRef](#)]
47. Podbolotov, K.B.; Dyatlova, E.M.; Volochko, A.T. Synthesis and reinforcement of heat-resistant cordierite-mullite ceramic structure with introduction of a fiber filler. *Refract. Ind. Ceram.* **2016**, *57*, 151–154. [[CrossRef](#)]
48. Grigoriev, S.; Peretyagin, P.; Smirnov, A.; Solis, W.; Diaz, L.A.; Fernandez, A.; Torrecillas, R. Effect of graphene addition on the mechanical and electrical properties of Al₂O₃-SiCw ceramics. *J. Eur. Ceram. Soc.* **2017**, *37*, 2473–2479. [[CrossRef](#)]
49. Grigoriev, S.N.; Volosova, M.A.; Okunkova, A.A.; Fedorov, S.V.; Hamdy, K.; Podrabinnik, P.A.; Pivkin, P.M.; Kozochkin, M.P.; Porvatov, A.N. Electrical Discharge Machining of Oxide Nanocomposite: Nanomodification of Surface and Subsurface Layers. *J. Manuf. Mater. Process.* **2020**, *4*, 96. [[CrossRef](#)]
50. Liu, Y.; Guo, Y.; Wang, L.; Zhang, Y.; Feng, Y. Effects of discharge status in AE-EDM of 8YSZ ceramic. *Procedia CIRP* **2020**, *95*, 488–493. [[CrossRef](#)]
51. Ji, R.; Liu, Y.; Zhang, Y.; Wang, F.; Cai, B.; Fu, X. Single discharge machining insulating Al₂O₃ stantaneous pulse energy in kerosene. *Mater. Manuf. Process.* **2012**, *27*, 676–682. [[CrossRef](#)]
52. Dashuk, P.N.; Kovtun, A.V.; Lukashenko, S.V.; Sokolov, B.N. The Method of Electrical Discharge Machining of Dielectrics. SU Patent 1 542 715 A1, 15 February 1990.
53. Kumar, M.; Vaishya, R.O.; Suri, N.M.; Manna, A. An Experimental Investigation of Surface Characterization for Zirconia Ceramic Using Electrochemical Discharge Machining Process. *Arab. J. Sci. Eng.* **2021**, *46*, 2269–2281. [[CrossRef](#)]
54. Raju, P.; Babasaheb, S. Study on analysis of plasma resistance variation in WEDM of insulating zirconia. *Mater. Manuf. Process.* **2021**, *36*, 59–72. [[CrossRef](#)]
55. Guo, Y.; Hou, P.; Shao, D.; Li, Z.; Wang, L.; Tang, L. High-Speed Wire Electrical Discharge Machining of Insulating Zirconia with a Novel Assisting Electrode. *Mater. Manuf. Process.* **2014**, *29*, 526–531. [[CrossRef](#)]
56. Shinde, B.; Pawade, R. Study on analysis of kerf width variation in WEDM of insulating zirconia. *Mater. Manuf. Process.* **2021**, *36*, 1010–1018. [[CrossRef](#)]
57. Hou, P.; Guo, Y.; Shao, D.; Li, Z.; Wureli, Y.; Tang, L. Influence of open-circuit voltage on high-speed wire electrical discharge machining of insulating Zirconia. *Int. J. Adv. Manuf. Technol.* **2014**, *73*, 229–239. [[CrossRef](#)]
58. Kostanovskiy, A.V.; Kostanovskaya, M.E.; Zeodinov, M.G.; Pronkin, A.A. Electrical resistivity of zirconium carbide at 1200–2500 K. *J. Phys. Conf. Ser.* **2021**, *1787*, 012008. [[CrossRef](#)]
59. Ordan'yan, S.S.; Zarichnyak, Y.P.; Bal'nova, E.S. Anomalous concentration dependences of thermal conductivity of ceramics in TiN-AlN and ZrC-ZrB₂ systems with the structure of “eutectics of rough conglomerate”. *Russ. J. Non-Ferr. Met.* **2014**, *55*, 92–96. [[CrossRef](#)]
60. Verma, S.; Satsangi, P.S.; Chattopadhyay, K.D. Enhancing process capabilities of electric discharge machining for nonconductive ceramics. *Proc. Inst. Mech. Eng. Part C J. Mech. Eng. Sci.* **2020**, *234*, 2402–2416. [[CrossRef](#)]
61. Hanaoka, D.; Fukuzawa, Y.; Yamashita, K. Research of large-area electrical discharge machining for insulating Si₃N₄ ceramics with the assisting electrode method. *Adv. Mater. Res.* **2014**, *939*, 76–83. [[CrossRef](#)]
62. Mohri, N. EDM of Advanced Ceramics—From Finish Machining to Machining Insulating Ceramics. *VDI Ber.* **1996**, *1276*, 289–296.
63. Muttamara, A.; Fukuzawa, Y.; Mohri, N.; Tani, T. Effects of structural orientation on EDM properties of sapphire. *Mater. Trans.* **2004**, *45*, 2486–2488. [[CrossRef](#)]
64. Li, X.; Liu, Y.; Yu, L.; Ji, R. Effects of electrical parameters on electrical discharge grinding of non-conductive engineering ceramics. *IET Conf. Publ.* **2006**, *524*, 1306–1309. [[CrossRef](#)]
65. Moudood, M.A.; Sabur, A.; Ali, M.Y.; Jaafar, I.H. Effect of Peak Current on Material Removal Rate for Electrical Discharge Machining of Non-Conductive Al₂O₃ Ceramic. *Adv. Mater. Res.* **2014**, *845*, 730–734. [[CrossRef](#)]
66. Kucukturk, G.; Cogun, C. A New Method for Machining of Electrically Nonconductive Workpieces Using Electric Discharge Machining Technique. *Mach. Sci. Technol.* **2010**, *14*, 189–207. [[CrossRef](#)]
67. Santos-Beltrán, A.; Gallegos-Orozco, V.; Estrada-Guel, I.; Bejar-Gómez, L.; Espinosa-Magaña, F.; Miki-Yoshida, M.; Martínez-Sánchez, R. TEM characterization of Al-C-Cu-Al₂O₃ composites produced by mechanical milling. *J. Alloy. Compd.* **2007**, *434–435*, 514–517. [[CrossRef](#)]
68. Volosova, M.A.; Okunkova, A.A.; Fedorov, S.V.; Hamdy, K.; Mikhailova, M.A. Electrical Discharge Machining Non-Conductive Ceramics: Combination of Materials. *Technologies* **2020**, *8*, 32. [[CrossRef](#)]
69. Vozniakovskii, A.A.; Kidalov, S.V.; Kol'tsova, T.S. Development of composite material aluminum-carbon nanotubes with high hardness and controlled thermal conductivity. *J. Compos. Mater.* **2019**, *53*, 2959–2965. [[CrossRef](#)]
70. Yuan, H.; Zhu, F.; Yang, B.; Xu, B.; Dai, Y. Latest progress in aluminum production by alumina carbothermic reduction in vacuum. *Zhenkong Kexue Yu Jishu Xuebao/J. Vac. Sci. Technol.* **2011**, *31*, 765–774.

71. Chaudhari, R.; Prajapati, P.; Khanna, S.; Vora, J.; Patel, V.K.; Pimenov, D.Y.; Giasin, K. Multi-Response Optimization of Al₂O₃ Nanopowder-Mixed Wire Electrical Discharge Machining Process Parameters of Nitinol Shape Memory Alloy. *Materials* **2022**, *15*, 2018. [[CrossRef](#)]
72. Ilani, M.A.; Khoshnevisan, M. An evaluation of the surface integrity and corrosion behavior of Ti-6Al-4 V processed thermodynamically by PM-EDM criteria. *Int. J. Adv. Manuf. Technol.* **2022**, *120*, 5117–5129. [[CrossRef](#)]
73. Sabur, A.; Mohammed Mehdi, S.; Ali, M.Y.; Maleque, M.A.; Moudood, A. Investigation of Surface Roughness in Micro-EDM of Nonconductive ZrO₂ Ceramic with Powder Mixed Dielectric Fluid. *Adv. Mater. Res.* **2016**, *1115*, 16–19. [[CrossRef](#)]
74. Wilkenhoener, R.; Buchkremer, H.P.; Stoeber, D.; Stolten, D.; Koch, A. Heat-resistant, electrically conducting joint between ceramic end plates and metallic conductors in solid oxide fuel cell. *Mater. Res. Soc. Symp.-Proc.* **1999**, *575*, 295–302. [[CrossRef](#)]
75. Pratas, S.; Silva, E.L.; Neto, M.A.; Fernandes, C.M.; Fernandes, A.J.S.; Figueiredo, D.; Silva, R.F. Boron Doped Diamond for Real-Time Wireless Cutting Temperature Monitoring of Diamond Coated Carbide Tools. *Materials* **2021**, *14*, 7334. [[CrossRef](#)] [[PubMed](#)]
76. Funke, V.F.; Yudkovskii, S.I.; Panov, V.S. Investigation of the physical properties and structure of TiC-WC-Co alloys. *Sov. Powder Metall. Met. Ceram.* **1962**, *1*, 449–454. [[CrossRef](#)]
77. Pyachin, S.A.; Burkov, A.A.; Makarevich, K.S.; Zaitsev, A.V.; Karpovich, N.F.; Ermakov, M.A. Optical characteristics of particles produced using electroerosion dispersion of titanium in hydrogen peroxide. *Tech. Phys.* **2016**, *61*, 1046–1052. [[CrossRef](#)]
78. Sahu, A.K.; Chatterjee, S.; Nayak, P.K.; Mahapatra, S.S. Study on effect of tool electrodes on surface finish during electrical discharge machining of Nitinol. *IOP Conf. Ser. Mater. Sci. Eng.* **2018**, *338*, 012033. [[CrossRef](#)]
79. Movchan, B.A.; Grechanyuk, N.I. Microhardness and microbrittleness of condensates of the TiC-Al₂O₃ system. *Inorg. Mater.* **1981**, *17*, 972–973.
80. Okunkova, A.A.; Volosova, M.A.; Kropotkina, E.Y.; Hamdy, K.; Grigoriev, S.N. Electrical Discharge Machining of Alumina Using Ni-Cr Coating and SnO Powder-Mixed Dielectric Medium. *Metals* **2022**, *12*, 1749. [[CrossRef](#)]
81. Grigor'ev, S.N.; Fedorov, S.V.; Pavlov, M.D.; Okun'kova, A.A.; So, Y.M. Complex surface modification of carbide tool by Nb + Hf + Ti alloying followed by hardfacing (Ti + Al)N. *J. Frict. Wear* **2013**, *34*, 14–18. [[CrossRef](#)]
82. Grigoriev, S.; Volosova, M.; Fyodorov, S.; Lyakhovetskiy, M.; Seleznev, A. DLC-coating application to improve the durability of ceramic tools. *J. Mater. Eng. Perform.* **2019**, *28*, 4415–4426. [[CrossRef](#)]
83. Volosova, M.; Grigoriev, S.; Metel, A.; Shein, A. The role of thin-film vacuum-plasma coatings and their influence on the efficiency of ceramic cutting inserts. *Coatings* **2018**, *8*, 287. [[CrossRef](#)]
84. Grigoriev, S.N.; Gurin, V.D.; Volosova, M.A.; Cherkasova, N.Y. Development of residual cutting tool life prediction algorithm by processing on CNC machine tool. *Mater. Werkst.* **2013**, *44*, 790–796. [[CrossRef](#)]
85. Grigoriev, S.N.; Kozochkin, M.P.; Sabirov, F.S.; Kutin, A.A. Diagnostic systems as basis for technological improvement. *Proc. CIRP* **2012**, *1*, 599–604. [[CrossRef](#)]
86. Grigoriev, S.N.; Sinopalnikov, V.A.; Tereshin, M.V.; Gurin, V.D. Control of parameters of the cutting process on the basis of diagnostics of the machine tool and workpiece. *Meas. Tech.* **2012**, *55*, 555–558. [[CrossRef](#)]
87. Viswanathan, V.; Laha, T.; Balani, K.; Agarwal, A.; Seal, S. Challenges and advances in nanocomposite processing techniques. *Mater. Sci. Eng. R* **2006**, *54*, 121–285. [[CrossRef](#)]
88. Wang, L.; Zhang, J.; Jiang, W. Recent development in reactive synthesis of nanostructured bulk materials by spark plasma sintering. *Int. J. Refract. Met. Hard Mater.* **2013**, *39*, 103–112. [[CrossRef](#)]
89. Zhang, Y.F.; Wang, L.J.; Jiang, W.; Chen, L.-D. Microstructure and properties of Al₂O₃-TiC composites fabricated by combination of high-energy ball milling and spark plasma sintering (SPS). *J. Inorg. Mater.* **2005**, *20*, 1445.
90. Grigoriev, S.N.; Volosova, M.A.; Okunkova, A.A.; Fedorov, S.V.; Hamdy, K.; Podrabinnik, P.A.; Pivkin, P.M.; Kozochkin, M.P.; Porvatov, A.N. Wire Tool Electrode Behavior and Wear under Discharge Pulses. *Technologies* **2020**, *8*, 49. [[CrossRef](#)]
91. Grigoriev, S.N.; Kozochkin, M.P.; Porvatov, A.N.; Volosova, M.A.; Okunkova, A.A. Electrical discharge machining of ceramic nanocomposites: Sublimation phenomena and adaptive control. *Heliyon* **2019**, *5*, e02629. [[CrossRef](#)]
92. Ay, M.; Etyemez, A. Optimization of the effects of wire EDM parameters on tolerances. *Emerg. Mater. Res.* **2020**, *9*, 527–531. [[CrossRef](#)]
93. Markopoulos, A.P.; Papazoglou, E.-L.; Karmiris-Obratański, P. Experimental Study on the Influence of Machining Conditions on the Quality of Electrical Discharge Machined Surfaces of aluminum alloy Al5052. *Machines* **2020**, *8*, 12. [[CrossRef](#)]
94. Moghaddam, M.A.; Kolahan, F. An optimised back propagation neural network approach and simulated annealing algorithm towards optimisation of EDM process parameters. *Int. J. Manuf. Res.* **2015**, *10*, 215–236. [[CrossRef](#)]
95. Grigoriev, S.N.; Volosova, M.A.; Okunkova, A.A.; Fedorov, S.V.; Hamdy, K.; Podrabinnik, P.A. Elemental and Thermochemical Analyses of Materials after Electrical Discharge Machining in Water: Focus on Ni and Zn. *Materials* **2021**, *14*, 3189. [[CrossRef](#)] [[PubMed](#)]
96. Grigoriev, S.N.; Teleshevskii, V.I. Measurement Problems in Technological Shaping Processes. *Meas. Tech.* **2011**, *54*, 744–749. [[CrossRef](#)]
97. Li, Y.; Zheng, G.; Cheng, X.; Yang, X.; Xu, R.; Zhang, H. Cutting performance evaluation of the coated tools in high-speed milling of AISI 4340 steel. *Materials* **2019**, *12*, 3266. [[CrossRef](#)] [[PubMed](#)]
98. Zakharov, O.V.; Brzhozovskii, B.M. Accuracy of centering during measurement by roundness gauges. *Meas. Tech.* **2006**, *49*, 1094–1097. [[CrossRef](#)]
99. Rezhnikov, A.F.; Kochetkov, A.V.; Zakharov, O.V. Mathematical models for estimating the degree of influence of major factors on performance and accuracy of coordinate measuring machines. *MATEC Web Conf.* **2017**, *129*, 01054. [[CrossRef](#)]

100. Zakharov, O.V.; Balaev, A.F.; Kochetkov, A.V. Modeling Optimal Path of Touch Sensor of Coordinate Measuring Machine Based on Traveling Salesman Problem Solution. *Procedia Eng.* **2017**, *206*, 1458–1463. [[CrossRef](#)]
101. Grigoriev, S.N.; Volosova, M.A.; Okunkova, A.A.; Fedorov, S.V.; Hamdy, K.; Podrabinnik, P.A. Sub-Microstructure of Surface and Subsurface Layers after Electrical Discharge Machining Structural Materials in Water. *Metals* **2021**, *11*, 1040. [[CrossRef](#)]
102. Fukuzawa, Y.; Tani, T.; Mohri, N. Machining characteristics of insulated Si₃N₄ ceramics by electrical discharge method—Use of powder-mixed machining fluid. *J. Ceram. Soc. Jpn.* **2000**, *108*, 184–190. [[CrossRef](#)]
103. Zhang, W.; Li, L.; Wang, N.; Teng, Y.L. Machining of 7Cr13Mo steel by US-PMEDM process. *Mater. Manuf. Process.* **2021**, *9*, 1060–1066. [[CrossRef](#)]
104. Calka, A.; Wexler, D. Mechanical milling assisted by electrical discharge. *Nature* **2002**, *419*, 147–151. [[CrossRef](#)] [[PubMed](#)]
105. Kumar, A.; Mandal, A.; Dixit, A.R.; Das, A.K. Performance evaluation of Al₂O₃ nano powder mixed dielectric for electric discharge machining of Inconel 825. *Mater. Manuf. Process.* **2018**, *33*, 986–995. [[CrossRef](#)]
106. Tzeng, Y.F.; Lee, C.Y. Effects of powder characteristics on electrodischarge machining efficiency. *Int. J. Adv. Manuf. Technol.* **2001**, *17*, 586–592. [[CrossRef](#)]
107. Liu, Y.H.; Li, X.P.; Ji, R.J.; Yu, L.L.; Zhang, H.F.; Li, Q.Y. Effect of technological parameter on the process performance for electric discharge milling of insulating Al₂O₃ ceramic. *J. Mater. Process. Technol.* **2008**, *208*, 245–250. [[CrossRef](#)]
108. Lin, Y.-J.; Lin, Y.-C.; Wang, A.-C.; Wang, D.A.; Chow, H.M. Machining characteristics of EDM for non-conductive ceramics using adherent copper foils. In *Advanced Materials Research, Materials Processing Technologies, Proceedings of the International Conference on Advances in Materials and Manufacturing Processes, Shenzhen, China, 6–8 November 2010*; Jiang, Z.Y., Liu, X.H., Bu, J.L., Eds.; Trans Tech Publications Ltd.: Durnten-Zurich, Switzerland, 2010. [[CrossRef](#)]
109. Panova, T.V.; Kovivchak, V.S. Formation of Oxide Layers on the Surface of Copper and its Alloys Modified by a High-Power Ion Beam. *J. Surf. Invest.* **2019**, *13*, 1098–1102. [[CrossRef](#)]
110. Murzin, S.P.; Kryuchkov, A.N. Formation of ZnO/CuO heterostructure caused by laser-induced vibration action. *Procedia Eng.* **2017**, *176*, 546–551. [[CrossRef](#)]
111. Silva, N.; Ramírez, S.; Díaz, I.; Garcia, A.; Hassan, N. Easy, Quick, and Reproducible Sonochemical Synthesis of CuO Nanoparticles. *Materials* **2019**, *12*, 804. [[CrossRef](#)]
112. Zheng, W.; Chen, Y.; Peng, X.; Zhong, K.; Lin, Y.; Huang, Z. The Phase Evolution and Physical Properties of Binary Copper Oxide Thin Films Prepared by Reactive Magnetron Sputtering. *Materials* **2018**, *11*, 1253. [[CrossRef](#)]
113. Ikim, M.I.; Spiridonova, E.Y.; Belysheva, T.V.; Gromov, V.F.; Gerasimov, G.N.; Trakhtenberg, L.I. Structural properties of metal oxide nanocomposites: Effect of preparation method. *Russ. J. Phys. Chem. B* **2016**, *10*, 543–546. [[CrossRef](#)]
114. Alkan, G.; Rudolf, R.; Bogovic, J.; Jenko, D.; Friedrich, B. Structure and Formation Model of Ag/TiO₂ and Au/TiO₂ Nanoparticles Synthesized through Ultrasonic Spray Pyrolysis. *Metals* **2017**, *7*, 389. [[CrossRef](#)]
115. Saikova, S.; Pavlikov, A.; Trofimova, T.; Mikhlin, Y.; Karpov, D.; Asanova, A.; Grigoriev, Y.; Volochaev, M.; Samoilo, A.; Zharkov, S.; et al. Hybrid Nanoparticles Based on Cobalt Ferrite and Gold: Preparation and Characterization. *Metals* **2021**, *11*, 705. [[CrossRef](#)]
116. Grigoriev, S.; Volosova, M.; Vereschaka, A.; Sitnikov, N.; Milovich, F.; Bublikov, J.; Fyodorov, S.; Seleznev, A. Properties of (Cr,Al,Si)N-(DLC-Si) composite coatings deposited on a cutting ceramic substrate. *Ceram. Int.* **2020**, *46*, 18241–18255. [[CrossRef](#)]
117. Guo, Y.; Zhu, T.; Zheng, J. Numerical simulation of electrical conductivity on the graphite-quartz model and its geophysical application. *Acta Geophys. Sin.* **2021**, *64*, 4031–4042.
118. Khvostov, V.V.; Khrustachev, I.K.; Minnebaev, K.F.; Zykova, E.Y.; Yurasova, V.E. Secondary particle emission from semiconductor crystals. *Vacuum* **2014**, *100*, 84–86. [[CrossRef](#)]
119. Galashev, A.E.; Ivanichkina, K.A.; Vorob'ev, A.S. Study of the Thermal Stability of a Monolayer SnS₂ Film on a Graphite Substrate. *High Temp.* **2021**, *59*, 66–72. [[CrossRef](#)]
120. Torres-Rojas, R.M.; Contreras-Solorio, D.A.; Hernández, L.; Enciso, A. Band gap variation in bi, tri and few-layered 2D graphene/hBN heterostructures. *Solid State Commun.* **2022**, *341*, 114553. [[CrossRef](#)]